# A Highly Miniaturized Satellite Payload Based on a Spatial Heterodyne Spectrometer for the Detection of Faint Emissions in the Atmosphere

Martin Kaufmann, Michael Deiml, Jilin Liu, Qiuyu Chen, Oliver Wroblowski, Martin Riese
Institute of Energy and Climate Research, Research Centre Juelich
Leo-Brandt-Str., 52428 Jülich, Germany; +49 2461 61 5250
m.kaufmann@fz-juelich.de

Friedhelm Olschewski, Ralf Koppmann
Institute for Atmospheric and Environmental Research, University of Wuppertal
Wuppertal, Germany

Klaus Mantel
Max-Planck-Institute for the Science of Light
Erlangen, Germany

Brian Solheim, Jinjun Shan, Gordon Shepherd
Department of Earth and Space Science and Engineering, York University
Toronto, Ontario, Canada

Tom Neubert
Central Institute for Engineering, Electronics and Analytics, Electronic Systems (ZEA-2), Research Centre Juelich
Leo-Brandt-Str., 52428 Jülich, Germany

Geshi Tan
Aerospace Flight Dynamics Laboratory
Beijing, China

**ABSTRACT**

A highly miniaturized limb sounder for the observation of faint emissions in the atmosphere is presented. The selected technology is a Spatial Heterodyne Spectrometer (SHS). The throughput of a SHS is orders of magnitude larger than of a conventional grating spectrometer of the same size. Its monolithic design makes it extremely robust against vibrations and shocks. It can be designed to deliver spectra at very high spectral resolution to resolve individual emission or absorption lines, or even Doppler shifts to derive winds. The small mass and low energy consumption makes SHS instruments particularly suitable for the deployment on nano-satellites or as secondary payloads on satellite constellations. In this presentation we introduce an instrument for the measurement of temperature in the mesosphere and lower thermosphere by observing the ro- vibrational structure of the $O_2$ atmospheric band at 762 nm in limb viewing geometry is presented. This instrument is suited to fly on a 3-6 unit CubeSat or as a secondary payload on a larger satellite.

## INTRODUCTION

For the study of faint signals, Fourier Transform Spectrometers (FTS) have significant advantages over conventional grating spectrometers. Their performance (throughput or etendue) is typically more than two orders of magnitude larger than grating spectrometers of the same size. A Spatial Heterodyne Spectrometer (SHS) is a special type of a FTS. It has no moving parts and can be build monolithic. Combined with 2-dimensional imaging detectors, it records the interferogram of the scene in one dimension and spatial information in the second dimension.

A group of German and Canadian research institutes and universities started an initiative to develop SHS instruments for remote sounding of the Earth atmosphere. Several instruments measuring in the ultraviolet, visible, or shortwave infrared are currently under development. This manuscript presents the basic design of an instrument to measure temperature in the mesosphere and lower thermosphere.

The most common technique to obtain temperatures in this region is to measure the emission of $CO_2$ in the mid infrared or to measure the absorption of sunlight by $CO_2$. Although the modeling of $CO_2$ emissions has its own problems regarding the determination of the non-local thermodynamic equilibrium state of the molecule, this method is well accepted and gives temperatures over a broad altitude range at a good signal to noise ratio.

Instruments measuring at infrared or longer wavelengths are quite large or high energy consuming, so that measurements in the ultraviolet/ visible/ near-infrared spectral regime are more appropriate for a nano- or microsat- platform. In this wavelength regime, mesospheric temperature measurements can be performed by the evaluation of the rotational distribution of molecular emission bands. The emitting states should be sufficiently long-lived, and the rotational distribution should be thermalized, such that it can be described by the kinetic temperature. It is best, if this emission is visible during day- and nighttime, such that temperatures can be obtained at all local times. The $O_2$ atmospheric band system fulfills all of these requirements. The strongest band within this system is the $O_2$ (0,0) atmospheric A-band at 762 nm, which was investigated in several studies[1, 2, 3, 4, 5]. Another advantage is that this temperature measurement technique builds upon relative intensity measurements. The requirements to monitor the radiometric performance of such kind of instrument are much more relaxed than for measurement strategies which rely on absolute intensities. It is also advantageous that the A-band emits at wavelengths below 1 µm, so that silicon-based detectors operating at ambient or moderately cooled conditions can be used for detection. This reduces the power consumption, mass, and costs of such an instrument significantly.

The main results presented in this paper are taken from the work of Kaufmann et al.[6] supplemented by some latest findings and general remarks about SHS.

## BASIC THEORY OF SPATIAL HETERODYNE SPECTROMETERS

In principle a SHS is a FTS, where the mirrors in each arm are replaced by diffraction gratings (Figure 1).

The incoming wavefront is separated at the beamsplitter and diffracted at the gratings, with a wavelength-dependent angle. The superposition of the two wavefronts then produces straight, parallel, and equidistant fringes with a spatial frequency depending on the wavelength of the light.

The zero frequency of the fringe pattern is at the Littrow wavelength and small wavenumber changes result in fringes with discernable, low spatial frequency, which can be observed with available imaging detectors.

The concept was originally proposed by Pierre Connes in a configuration called “Spectromètre interférential à selection par l’amplitude de modulation (SISAM)”[7]. With the advent of imaging detectors, this idea was taken up by, e.g., [8, 9, 10, 11, 12, 13, 14, 15, 16, 17].

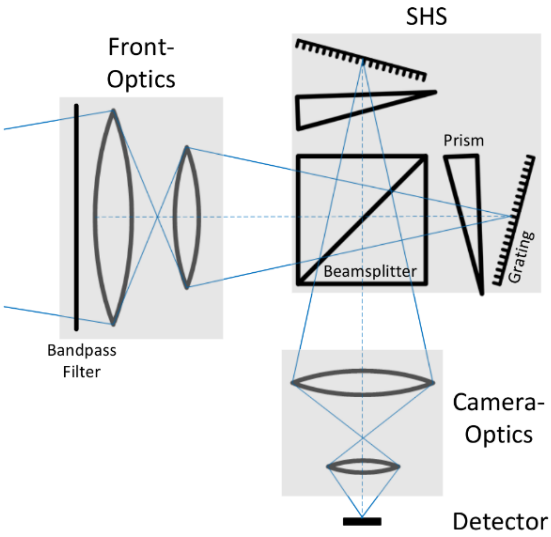


**Figure 1. Principle design of the SHS with front and detector optics**

The design of a SHS for a particular wavelength and spectral resolution follows a few simple relations, which are shortly summarized to illustrate the main characteristics of this device. For a derivation of the mathematical expressions see, e.g., [18, 19, 10], and references cited therein. The tilt angle of the gratings with respect to the optical axis is called Littrow angle $\Theta_L$. Light at the Littrow wavenumber $\sigma_L$ is returned in the same direction as the incoming path, as described by the grating equation (for diffraction order one and grating groove density1/d:

$$\sigma_L = \frac{1}{2d \sin \Theta_L}$$

Combining the intensity equation of a conventional FTS and the grating equation for small incident angles at the grating gives the SHS equation for ideal conditions, relating the incoming radiation at wavenumber σ to the spectral density at position x parallel to the dispersion plane. The heterodyned fringe frequency κ is:

$$\kappa = 4 \tan \Theta_L (\sigma - \sigma_L)$$

The maximum resolving power of a SHS is nearly proportional to the number of grating grooves illuminated by the incoming beam. The bandpass of a SHS is limited by the detector resolution due to the Nyquist theorem.

As for conventional FTS or Fabry-Perot instruments, the acceptance angle of light for a conventional SHS is inversely proportional to its resolving power[18]. The acceptance angle of a SHS can be increased significantly, if prisms are inserted into the two interferometer arms. The prisms rotate the image of the gratings so that they appear to be located in a common virtual plane which is oriented perpendicular to the optical axis for a wide range of incident angles. At the end, the acceptance angle of the SHS including field widening prisms is only limited by spherical aberration for systems with small Littrow angles and astigmatism for large Littrow angles[20]. Depending on the actual design, the prisms increase the etendue or throughput of a SHS by 1-2 orders of magnitude.

A general advantage of SHS are the relaxed alignment tolerances, because in most optical setups the gratings are imaged onto a focal plane array. As a result, each detector pixel sees only a small area of the optical elements, so that moderate misalignments or inaccuracies in the surface quality affect limited spatial regions on the detector, only. This means that the interferogram is distorted locally rather than reduced in contrast. SHS can be realized using transmitting or all-reflecting elements. SHS using dispersive elements can be built monolithically, making them very robust for harsh environments, e.g. during rocket launches.

## BACKGROUND ON TEMPERATURE MEASUREMENTS BY MEANS OF $O_2$ A-BAND OBSERVATIONS

Here, atmospheric temperature is derived from the measurement of the rotational structure of the $O_2$ atmospheric band system. Light emitted in this system stems from emissions of the $O_2(b^1\Sigma_g^+)$ electronically excited state. An overview of the chemistry and molecular dynamics of excited $O_2$ is given by, e.g., [5] and references cited therein. All excitation processes of $O_2(b^1\Sigma_g^+)$ except one require sunlight. The only nighttime excitation process is chemiluminescence called the 2-step Barth process[21, 22]. There are three absorption bands in this system (A, B, and γ bands). All of these bands end up in a vibrational ground state. None of these bands can be observed from the ground, because of the high abundance of ground state molecular oxygen molecules in the atmosphere. The radiative lifetime of the $O_2(b^1\Sigma_g^+)$ is about 12 seconds. This long lifetime assures that the molecule is in rotational equilibrium with the ambient atmosphere, such that rotational and ambient temperature are identical.

The spectral shape of the A-band around 762 nm for two different temperatures (for 200 K and 210 K) is illustrated in Figure 2. The spectra in the upper panel have been normalized to show identical band intensities. The light gray area shows their intensities (multiplied by a factor of 10) as seen from an instrument with a spectral resolution of 0.1 nm. The dashed line is the filter transmission curve of the instrument presented later. The dotted vertical line is drawn at the Littrow wavelength. The percentage difference of the line intensities are shown in the lower panel; the symbol size scales with the absolute intensity of the lines. It is clearly visible from the figure that higher temperatures give a flatter spectrum. A 10 K change in temperature affects the rotational distribution of strong emission lines at 760-765 nm between ±6%. This means that the band structure must be measured better than 1% to derive temperatures with a precision of 1.5 K.

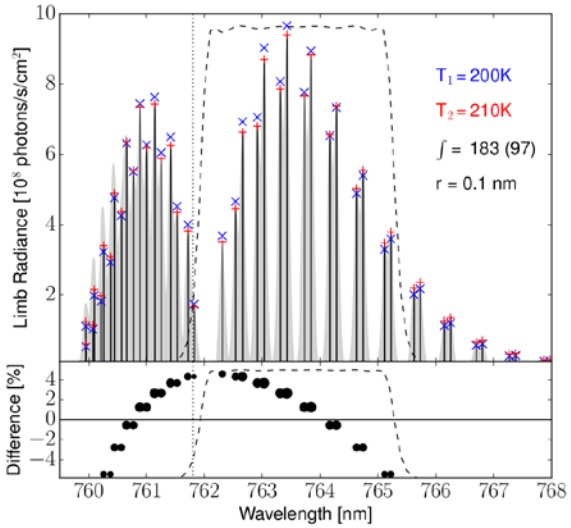


**Figure 2. $O_2$ A-band limb emission line calculations assuming a global temperature of 200 K and 210 K (upper panel). The percentage difference of the line intensities at 200 K and 210 K are shown in the lower panel**

## DESIGN PARAMETERS OF THE SHS LIMB SOUNDER FOR THE OBSERVATION OF $O_2$ A-BAND EMISSSIONS IN THE MESOPAUSE REGION

The goal was to design a SHS limb sounder to measure (part of) the $O_2$ A-Band spectrum at 762 nm. The requirements on the spectral resolution and the spectral bandpass were determined by simulation studies optimizing the retrieved atmospheric temperature accuracy and precision. Boundary conditions are the size of the instrument (shall fit into a volume of 1-2 litres excluding a straylight baffle), the usage of as many commercial off the shelf (COTS) components as possible, the detector size and pixel number (full HD, 5 µm pitch), and a field of view of 1.3°.

An integral part of a SHS design is the optical filter located between the SHS and the scene to be observed. For this instrument, a six cavity design bandpass filter with a center wavelength of 763.6 nm and a bandwidth of 3.3 nm was chosen. Since a SHS instrument maps the spectrum on both sides of the Littrow wavelength symmetrically into Fourier space, the filter must be adapted in such a way that there is no overlap of lines from different sides of the Littrow wavelength in the interferogram. In our design, the Littrow wavelength is at 761.8 nm, e.g. the filter blocks most of the radiance from the shorter wavelength side of the Littrow wavelength. The purpose of the front optics is to image a scene at the Earth's limb onto the gratings. The detector optics images the gratings onto the focal plane of the 2-dimensional detector. The image at the detector contains spatial information about the scene in both dimensions. An interferogram is superimposed on this scene in the direction perpendicular to the grating grooves. For the instrument presented in this work, the gratings are oriented in such a way that the interferogram spans over the horizontal direction, assuming that intensity fluctuations in the horizontal direction are small or smeared out during the exposure of the image compared to the modulation depth of the interferogram, which is valid in atmospheric limb sounding.

The front-optics (Figure 3) consists of four lenses, which image an object at infinity of an angular extent of 1.3° onto a circle of a diameter of 7 mm on the virtual image of the gratings. This corresponds to a theoretical spectral resolution of about 16,800. The clear aperture diameter of the front lens is 66 mm and the distance between the first lens and the SHS is 104 mm. The etendue of this configuration is 0.014 $cm^2$ sr. The detector optics images the active area of the gratings onto the detector and consists of lenses as well. The magnification is 0.55, i.e. the illuminated area at the detector has a diameter of about 3.8 mm. This value was chosen as a trade-off between the form factor required and the desired spectral and spatial resolution. The distance between the beam splitter and the detector focal plane is 46 mm.

The detector chosen for this instrument is a low noise silicon-based CMOS image sensor. The optical format is 2/3 (9.7 mm x 5.4 mm) and the pixel size is 5 µm x 5 µm, resulting in 1920 x 1080 pixels in total, from those 840 x 840 pixels are used here. The quantum efficiency of this detector is about 0.4 at 760 nm.

Like the SHS, the entire optical system was optimized using optical raytracing software. The wave front peak-to-valley extension of the optical system is less than a half wavelength for center rays and one wavelength at maximum for the edge region of the field.

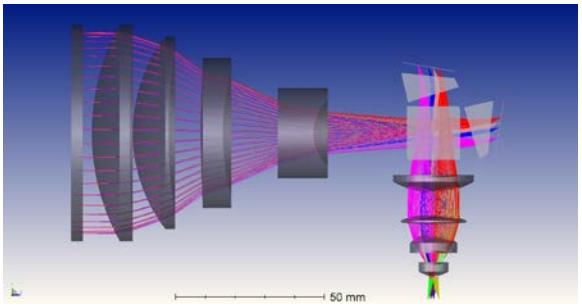


**Figure 3. Optical components of the instrument, including the interference filter, the front optics, the SHS, the detector optics and the detector.**

The extension of the point spread function is 5 µm for inner and 10 µm for outer pixels, which does not deteriorate the determination of the different waves in the interferogram, because the highest spatial frequency to be observed corresponds to a wavelength of about 45 µm. For the designed temperature range (20°C), the modular transfer function (MTF) is always larger than 85% and drops down to 50% at -10°C in the worst case (for highest spatial frequencies and marginal rays). The three core components (SHS, front- and camera optics) are illustrated in Figure 4. The SHS as well as the optical structure were built in-house.

**Figure 4. SHS, front- and detector optics**

The optical instrument is complemented by a readout electronics developed at Central Institute for Engineering, Electronics and Analytics, Electronic Systems (ZEA-2) of Research Centre Jülich. It consists of two boards, the PXE (proximity electronics) for directly interfacing to different detectors and the FEE (frontend electronics). Its tasks are to acquire the detector data, provide data preprocessing (data binning), process housekeeping data, and provide an interface to the satellite bus. The FEE is based on a System on a Chip (SoC) with ARM cores and FPGA fabric. The current version of the FEE communicates via CAN- and a binary

LVDS bus. The data rates of the instrument depend on integration time and pixel binning and range from 3kByte/s to 100 kByte/s. Most of the components are COTS. Therefore the electronics as well as the detector were tested with a Co-60 radiation source up to 100 krad(Si). Without any shielding, the ZYNQ SoC module failed at a total ionizing dose (TID) of 12 krad and first failures of the bus drivers appeared at 25-30 krad. The COTS CMOS detector survived up to 85 krad. This means that this system should work for a 3-year low-Earth satellite mission, if a 3mm Al shielding is applied.

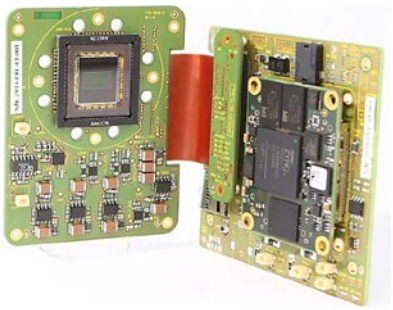

**Figure 5. Proximity- and frontend electronics**

An engineering model of the entire instrument including a straylight baffle (filling about 50% of the entire volume) and a passive cold radiator on top of the instrument is shown in Figure 6. In a concept study[23] an extendable baffle was designed such that the total length of the entire instrument is about 15 cm, only.

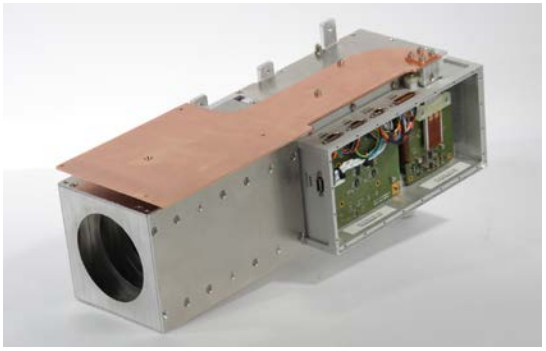

**Figure 6. Engineering model of the $O_2$ A-Band limb sounder including a straylight baffle**

## EXPECTED INSTRUMENT PERFORMANCE

In theory, SHS spectral resolution is diffraction limited by the grating. The designed resolving power of our $O_2$ A-Band SHS is about 16.800. Variations of the phase and the contrast of the interferogram across the focal plane as well as windowing associated to Fourier transformation reduce this value by some ten percent. Therefore, further performance assessment assumes that the effective spectral resolution of this instrument is 10,000.

To assess the radiometric performance, nighttime conditions are assumed, because the atmospheric signal is at least one order of magnitude larger for daytime conditions. A calculated nighttime interferogram as seen from this instrument is illustrated in Figure 7. Highest intensities are seen around 90 km altitude in the $O_2$ A-Band nighttime layer maximum.

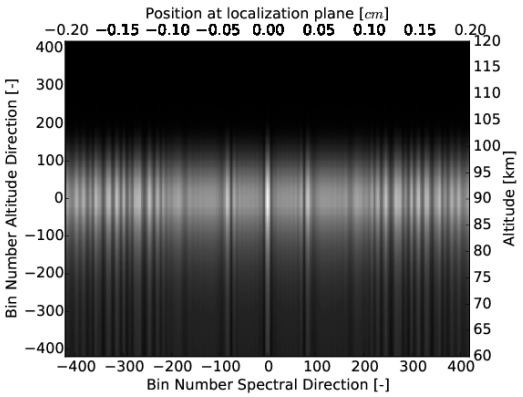


**Figure 7. Calculated nighttime limb sounding interferogram**

To determine the expected signal-to-noise ratio of the instrument for a given integration time, we estimate the amount of incoming light, which is available in the modulated part of the interferogram and the noise of the detector. In a SHS, 50% of the incoming radiation are lost at the beam splitter. The holographic gratings used have an efficiency of about 2/3 at 762 nm, so that another 1/3 of the radiation is not available in the modulated part of the radiance. Misalignments and aberrations of optical components are estimated to reduce the contrast of the interferogram, so that we expect to detect about 20% of the incoming radiation in the modulated part of the interferogram.

The noise of the signal is, by far, limited by shot noise, which scales with the square root of the (electrical) signal. The latter consists of the electrons excited by the signal of interest and the dark current caused by thermal processes. The detector selected for an instrument demonstrator has a dark current corresponding to 5-10 photons/pixel at 20°C, which is a factor of 10-20 lower than the atmospheric signal at the nighttime $O_2$ A-Band

mesospheric emission layer maximum and therefore it not a dominant source of random noise at these altitudes. Further study shows[6] that to obtain temperatures with a precision of 2~K at a vertical resolution of 2-3 km, typical integration times will be in the order of one minute, which is similar to the performance of earlier but significantly larger instruments[6].

## PRO AND CONS OF THE SHS TECHNOLOGY

The application of an SHS for the observation of $O_2$ A-Band emissions takes full advantage of this spectrometer concept. The main one is to obtain a monolithic highly miniaturized device with outstanding light gathering power and high spectral resolution. The use of dispersive elements makes it relatively inexpensive and easy to assemble, if appropriate alignment tools are available. For the selected and many other applications, the interferometer nature of SHS has inherent advantages due to multiplexing by increasing the signal-to-noise ratio of a shot-noise limited detector, which is increasing with the square-root of the total signal. However, multiplexing becomes a disadvantage, if the signal of interest is low compared to other signals within the bandpass of the instrument, as it is the case, for example, for the detection of absorption lines – at least for shot-noise limited systems. This can possibly be compensated by the extraordinary throughput of SHS due to field widening, but this depends on the actual application.

## SUMMARY

We presented a design for a highly miniaturized instrument to obtain mesospheric temperatures. A spatial heterodyne spectrometer is used to measure the rotational structure of the $O_2$ A-band, which is complemented by fore- and detector optics. The size of the entire instrument including a straylight baffle is around 3.5 litres, the mass is less than 5 kilograms, and the power consumption is about 6 W. The instrument can deliver temperatures at a 2 K precision for an integration time of about one minute for nighttime and a few seconds for daytime conditions.

A prototype version of this instrument was tested in March 2017 on a sounding rocket by a student team[24]. The instrument survived the rocket launch and worked nominally. Unfortunately, it was not possible to record limb spectra with a stable attitude due to a failure of the detumbling mechanism of the rocket.

The next step in this project is the advancement of this instrument for an in-orbit verification on a satellite. The main requirements on a satellite platform are a stable line-of-sight attitude, which should be a few arc minutes for the time of an image acquisition[25]. The control of that angle could be an order of magnitude less precise, since it can be compensated to some degree by an extended vertical field of view of the instrument.

From a technological perspective, advancement of the SHS assembly procedure with the aim of a small scale production of SHS for satellite constellations or other applications is highly desirable. The current SHS is glued together with optical cement and a high degree of manual work, which includes the construction of an individual alignment device. Atomic bonding is a very promising technology to obtain SHS with higher tolerances, minimum spread between samples and lower costs per item.

## REFERENCES


1. Rodrigo, R., J. Lopez-Moreno, M. Lopez-Puertas, and A. Molina, “Analysis of OI-557.7 nm, NAD, OH(6-2) and $O_2$(1εg+) (0-1) nightglow emission from ground-based observations,” Journal of Atmospheric and Terrestrial Physics, vol. 47, no. 11, pp. 1099–1110, 1985.
2. Torr, M.R., D. G. Torr, and R. R. Laher, “The $O_2$ atmospheric 0-0 band and related emissions at night from SPACELAB 1,” Journal of Geophysical Research: Space Physics, vol. 90, no. A9, pp. 8525–8538, 1985.
3. McDade, I. C. and E. J. Llewellyn, “The excitation of O($^1$S) and $O_2$ bands in the nightglow: a brief review and preview,” Canadian Journal of Physics, vol. 64, no. 12, pp. 1626–1630, Dec. 1986.
4. Meriwether, J. W., “A review of the photochemistry of selected nightglow emissions from the mesopause,” Journal of Geophysical Research: Atmospheres, vol. 94, no. D12, pp. 14629–14646, 1989.
5. Slanger, T. G. and R. A. Copeland, “Energetic oxygen in the upper atmosphere and the laboratory,” Chemical Reviews, vol. 103, no. 12, pp. 4731–4766, 2003.
6. Kaufmann, M., F. Olschewski, K. Mantel, B. Solheim, G. Shepherd, M. Deiml, J. Liu, R. Song, Q. Chen, O. Wroblowski, D. Wei, Y. Zhu, F. Wagner, F. Loosen, D. Froehlich, T. Neubert, H. Rongen, P. Knieling, P. Toumpas, J. Shan, G. Tang, R. Koppmann, and M. Riese, “A highly miniaturized satellite payload based on a spatial heterodyne spectrometer for atmospheric temperature measurements in the mesosphere and lower thermosphere,” Atmospheric Measurement Techniques Discussions, vol. 2018, pp. 1–19, 2018. [Online]. Available: https://www.atmos-meas-tech-discuss.net/amt-2017-437/

7. Connes, P., “Spectrometre interferentiel Ã selection par l‘amplitude de modulation,” J. Phys.Radium, vol. 19 (3), pp. 215–222, 1958.

8. Harlander, J. M. and F. L. Roesler, “Spatial heterodyne spectroscopy: a novel interferometric technique for ground-based and space astronomy,” Proc.SPIE, vol. 1235, 1990.

9. Douglas, N. G., “Heterodyned holographic spectroscopy,” Publications of the Astronomical Society of the Pacific, vol. 109, no. 732, p. 151, 1997.

10. Smith, B. W. and J. M. Harlander, “Imaging spatial heterodyne spectroscopy: theory and practice,” Proc.SPIE, vol. 3698, 1999.

11. Watchorn, S., F. L. Roesler, J. M. Harlander, K. P. Jaehnig, R. J. Reynolds, and W. T. Sanders, “Development of the spatial heterodyne spectrometer for UV remote sensing of the interstellar medium,” Proc.SPIE, vol. 4498, 2001.

12. Harris, W. M., F. L. Roesler, J. Harlander, L. Ben-Jaffel, E. Mierkiewicz, J. Corliss, and R. J. Oliversen, “Applications of reflective spatial heterodyne spectroscopy to UV exploration in the solar system,” Proc.SPIE, vol. 5488, 2004.

13. Roesler, F. L., “An overview of the SHS technique and applications,” in Fourier Transform Spectroscopy/ Hyperspectral Imaging and Sounding of the Environment. Optical Society of America, 2007.

14. Englert, C. R., M. H. Stevens, D. E. Siskind, J. M. Harlander, and F. L. Roesler, “Spatial heterodyne imager for mesospheric radicals on stpsat 1,” Journal of Geophysical Research: Atmospheres, vol. 115, no. D20, 2010.

15. Watchorn, S., F. L. Roesler, J. Harlander, K. P. Jaehnig, R. J. Reynolds, and W. T. Sanders, “Evaluation of payload performance for a sounding rocket vacuum ultraviolet spatial heterodyne spectrometer to observe 1550 emissions from the cygnus loop,” Appl. Opt., vol. 49, no. 17, pp. 3265–3273, Jun 2010.

16. Bourassa, A. E., J. Langille, B. Solheim, D. Degenstein, and F. Dupont, “The spatial heterodyne observations of water (show) instrument for high resolution profiling in the upper troposphere and lower stratosphere,” in Light, Energy and the Environment. Optical Society of America, 2016.

17. Lenzner M., and J.-C. Diels, “Concerning the spatial heterodyne spectrometer,” Opt. Express, vol. 24, no. 2, pp. 1829–1839, Jan 2016.

18. Harlander, J. M., “Spatial Heterodyne Spectroscopy: Interferometric Performance at any Wavelength Without Scanning.” Ph.D. dissertation, The University of Wisconsin - Madison., 1991.

19. Cooke, B.J., B. W. Smith, B. E. Laubscher, P. V. Villeneuve, and S. D. Briles, “Analysis and system design framework for infrared spatial heterodyne spectrometers,” Proc.SPIE, vol. 3701, 1999.

20. Harlander, J.M., R. J. Reynolds, and F. L. Roesler, “Spatial heterodyne spectroscopy for the exploration of diffuse interstellar emission lines at far-ultraviolet wavelengths,” Astrophysical Journal, Part 1, vol. 396, pp. 730–740, Sep. 1992.

21. Barth C.A., and A. F. Hildebrandt, “The 5577 a airglow emission mechanism,” Journal of Geophysical Research, vol. 66, no. 3, pp. 985–986, 1961.

22. Barth, C.A., “Upper atmosphere three-body reactions study leading to light emission with laboratory results applied to night airglow,” NASA Technical Report, no. 19650033531, 1964.

23. Deiml, M., M. Kaufmann, P. Knieling, F. Olschewski, P. Toumpas, M. Langer, M. Ern, R. Koppmann, and M. Riese, “DISSECT-development of a small satellite for climate research,” Proceedings of the 65th International Astronautical Congress, Toronto, Canada, no. IAC-14,B5,1,10,x22911, 2014.

24. Deiml,M., R. Song, D. Fröhlich, B. Rottland, F. Wagner, J. Liu, O. Wroblowski, Q. Chen, F. Loosen, M. Kaufmann, H. Rongen, T. Neubert, H. Schneider, F. Olschweski, P. Knieling, K. Mantel, B. Solheim, G. Shepherd, R. Koppmann, and M. Riese, “Test of a remote sensing fourier transform interferometer for temperature measurements in the mesosphere on a rexus rocket,” Proceedings of the 23rd ESA Symposium on European Rocket and Balloon Programmes and Related Research, Visby, Sweden, 2017.

25. Kaufmann, M., M. Deiml, F. Olschewski, K. Mantel, F. Wagner, F. Loosen, D. Fröhlich, H. Rongen, T. Neubert, B. Rottland, H. Schneider, M. Riese, P. Knieling, J. Liu, R. Song, O. Wroblowski, Q. Chen, R. Koppmann, B. Solheim, J. Shan, and G. Shepherd, “A miniaturized satellite payload hosting a spatial heterodyne spectrometer for remote sensing of atmospheric temperature,” Proceedings of the 11th IAA Symposium on Small Satellites for Earth Observation, Berlin, Germany, 2017.